Twinning-induced dislocation and coordinated deformation behavior of a high-Nb TiAl alloy during high-cycle fatigue

Xuesong Xu [a,b], Hongsheng Ding [a,], Haitao Huang [a], He Liang [a], R. V. Ramanujan [b], Ruirun Chen [a], Jingjie Guo [a], Hengzhi Fu [a]*

[a] National Key Laboratory for Precision Hot Processing of Metals, School of Materials Science and Engineering, Harbin Institute of Technology, Harbin 150001, China

[b] School of Materials Science and Engineering, Nanyang Technological University, 50 Nanyang Avenue, Singapore 639798, Singapore

* Corresponding author.
Email address: dinghsh@hit.edu.cn (H. Ding)

Abstract

The deformation mechanism responsible for the high-cycle rotating bending fatigue of a high-Nb TiAl alloy was investigated. Fatigue deformation in the γ phase was dominated by superlattice dislocations [$01\bar{1}$] and twinning. Dislocations <110> in the B2 phase can be induced by twins in the adjacent γ phase, which has a low stacking fault energy owing to the high Nb content. Stress transfer between two adjacent phases can be accomplished through atomic rearrangement of the interface by twinning. The local stresses were accommodated by the continuous dislocation slip of the B2 phase, deformation twins, and twin intersections in the γ phase.

Keywords: TiAl alloy, fatigue, twinning, dislocation, coordinated deformation

1. Introduction

TiAl-based alloys have a broad range of applications in the aerospace field owing to their low density, high specific strength, excellent high-temperature properties, large elastic modulus, good oxidation resistance, and high creep resistance [1,2]. The GEnx™ engine was the first commercial aircraft engine to use TiAl alloys (Ti-48Al-2Cr-2Nb) as a low-pressure turbine (LPT) blade. Subsequently, Ti-43.5Al-4Nb-1Mo-0.1B (TNM) alloys were used as LPT blades for the manufacture of PW1100G™ engines [3]. To further improve the engineering performance of these alloys at high temperatures, β stabilizing elements such as Nb, W, Cr, and V can be added [4,5]. High-Nb containing TiAl alloys with high strength and elevated maximum service temperature are typical representatives of a new generation of TiAl alloys [6,7]. However, excessive β stabilizer content can produce a large amount of hard and brittle B2 phase at room temperature. This may provide a preferential fracture initiation and growth path [8], significantly impacting both the room- and elevated-temperature mechanical properties [9-11]. Therefore, it is vital to optimize the microstructure of advanced multicomponent TiAl alloys by tuning the alloy composition and processing parameters, particularly with respect to the control of the B2 phase.

Because all engineering applications of TiAl alloys involve components subjected to fluctuating or cyclic loads, fatigue properties must be considered to evaluate the service life of TiAl alloys. Numerous studies on dual-phase TiAl alloys have focused on fatigue fracture and deformation behavior. Near or fully lamellar microstructures show substantially higher fatigue resistance, compared with duplex or equiaxed gamma microstructures [12]. For the multiphase TiAl alloy, Dahar *et al.* [13,14] determined the fatigue performance of the TNM alloy at room temperature and found that the TNM alloy exhibited lower fracture resistance compared with the cast Ti-48Al-2Cr-2Nb alloy. Signori *et al.* [15] also investigated the effect of the volume fraction of the β/γ duplex structure on fatigue crack growth behavior of a Ti-43Al-4Nb-5V alloy. They revealed that the presence of the β phase associated with γ grains in a TiAl alloy increases the stress intensity threshold and decreases the Paris slope compared with the corresponding duplex TiAl alloy. Sakaguchi [16] studied the temperature-dependent fatigue behavior of β containing TiAl alloys and pointed out that the higher fatigue resistance of the triplex (α_2/γ lamellar colonies and β/γ duplex phases) microstructure at high temperatures is mainly due to the larger volume fraction of the ductile β phase. Therefore, the fatigue properties of the new-generation TiAl alloys are significantly different from those of traditional dual-phase TiAl alloys owing to the existence of the

B2 phase. It is important to explore the role of the B2 phase in the fatigue deformation process of multiphase high-Nb TiAl alloys.

The mechanical behaviors of high-Nb TiAl alloys, such as tensile, compressive, creep, and low-cycle fatigue properties, have been previously studied [17-19]. Most studies have focused on the deformation behavior of the α_2 and γ lamellae [20,21]. Hoppe *et al.* [21] investigated the internal stress arising from misfitting α_2/γ lamellar interfaces, the lack of independent slip systems and the elasto-plastic co-deformation of different alloy constituents, which can act as constant long-range retarding forces that impede dislocation motion. Edwards *et al.* [22] pointed out that the multi-scale combination of several transverse twinning systems on different {111} planes in γ-TiAl lamellae can relieve the elastic stresses generated at the lamellar interface by the primary (highest Schmid factor) twinning system. Song *et al.* [23] studied the deformation and phase transformation behavior of the α_2 phase in a TiAl alloy and found that the twin-like morphology in the α_2 phase was due to the {1011}<1012> deformation twinning mode. The twin interfaces of α_2 can serve as preferential sites for ω_o phase nucleation. With an increase in the β-stabilizing element content, the deformation behavior of the B2 phase must be considered. Kolb *et al.* [24] studied the deformation of the B2 phase of a Ti-44.5Al-6.25Nb-0.8Mo-0.1B alloy after nanoindentation tests at room and high temperatures. They found that the deformation in the B2 phase (at 25℃ and 600℃) was mainly caused by dislocation slipping with <111>-type Burgers vector. Liu *et al.* [25] studied the tensile deformation behavior of a Ti-42Al-6V-1Cr alloy and found that when deformed below 700 °C, <110>-type dislocations were active in B2 grains. When deformed at 800 °C, <111>, <110>, and <100>-type dislocations were active, and more slip modes would lead to softening. However, the B2 phase is not isolated in this alloy. Its co-deformation behavior with other adjacent phases, which is of great significance for understanding and predicting the process of alloy crack nucleation and premature fracture, has not been investigated. Thus, the deformation mechanism of the B2 and γ phases in multiphase high-Nb TiAl alloys has not yet been studied in detail.

The Ti46Al7Nb0.4W0.6Cr0.1B alloy was prepared using the electromagnetic cold crucible directional solidification method, and its microstructure and high-cycle rotating-bending fatigue properties were characterized and evaluated. In addition, the coordinated deformation mechanism of this multiphase high-Nb TiAl alloy is discussed in detail. The novelty of this study is the development of a microalloyed high-Nb TiAl alloy with good fatigue properties and elucidation of its coordinated deformation

behavior. The significance of this finding is that it provides valuable insights pertaining to the coordinated deformation behavior of multiphase materials, especially for fcc/bcc-based microstructures.

2. Material and Methods

A microalloyed high-Nb TiAl master alloy was investigated in this study, with a nominal composition of Ti46Al7Nb0.4W0.6Cr0.1B (at. %). It was prepared via vacuum consumable melting and induction skull melting. The actual chemical composition of the TiAl ingot was measured as Ti-45.89 at. %Al-7.08 at. %Nb-0.44 at. %W-0.63 at. %Cr-0.11 at. %B using the inductively coupled plasma atomic emission spectrometry (ICPAES) method. Round bars with a diameter of 20 mm were cut from the master alloy using wire electrical discharge machining (EDM). Subsequently, they were further processed by electromagnetic cold crucible directional solidification, which was carried out under a high-purity argon atmosphere with a power of 45 kW and a pulling rate of 8.3 μm/s. The directional solidification (DS) process and the macrostructure have been reported in a previous study [26].

The high-cycle rotating bending fatigue tests were carried out on a H-7 rotating bending fatigue testing machine (Shimadzu, Japan) (Fig. 1(a)), with a rotational speed of 3000 rev/min, $K_t = 1$, and R = -1. The samples were taken from the middle of the directionally solidified sample, cut, ground and polished to ensure that the average roughness Ra of the surface was less than 0.2 μm. The rotating bending fatigue specimen was funnel-shaped (Fig. 1(b)). In addition, the minimum section size was Φ6 mm and 30 mm in length of the gauge region, and the total length was 90 mm.

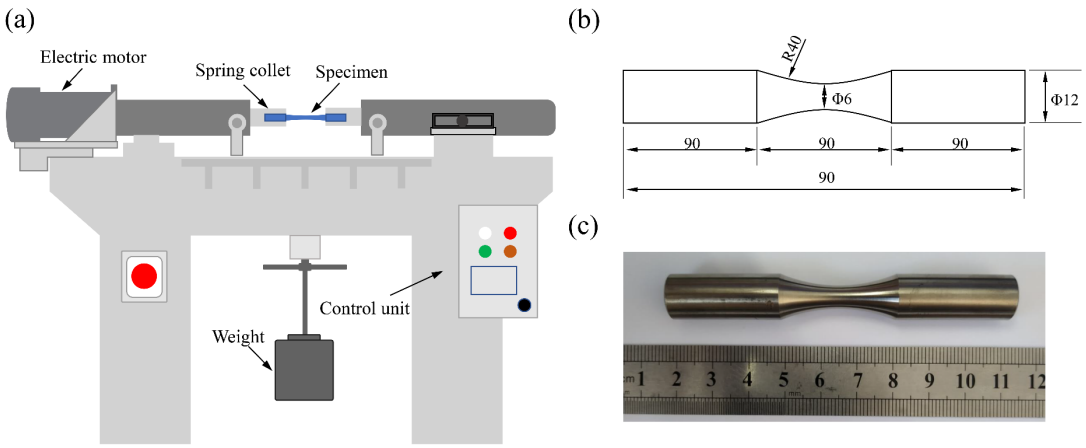

Fig. 1 (a) Schematic diagram of rotating bending fatigue equipment; (b) Specimen geometry; (c) Image of the specimen.

The microstructure was analyzed using a JAX-8230 (JEOL, Japan) electron probe microanalyzer (EPMA) with a wavelength dispersive spectrometer (WDS) attachment. Samples used for microstructural characterization were first ground with SiC abrasive papers, and then were subjected to the electrolytic polished method in a solution of 5% $HClO_4$ + 35% butanol + 60% methanol (in volume fraction) at 30 V and -25℃. The average volume fraction values were calculated using quantitative image analysis data from 15 digitalized scanning electron microscopy (SEM) images. The transmission electron microscopy (TEM) samples were cut along the middle cross-sectional direction of the run-out funnel-shaped sample after fatigue testing, mechanically ground to 50 μm, and thinned using an ion beam thinner (GATAN695, USA) with ionized argon. TEM analysis was performed using a Talos F200X (FEI, USA) microscope with energy-dispersive X-ray analysis (EDX). Scanning transmission electron microscopy (STEM) and high-resolution TEM (HRTEM) were employed for more detailed microstructural investigation. The Burgers vectors $\boldsymbol{b}$ were determined using different diffraction vectors $\boldsymbol{g}$ and by applying the $\boldsymbol{g}\cdot\boldsymbol{b}$ criterion [27].

3. Results and Discussion

3.1 Microstructure of the microalloyed high-Nb TiAl alloy

Fig. 2 shows the SEM images and EPMA-WDS mapping results for the Ti46Al7Nb0.4W0.6Cr0.1B alloy. The alloy was composed of α_2/γ lamellae, short rod-shaped boride phases, a bright white B2 phase, and a dark blocky γ phase distributed between and inside the lamellar colonies. The principle of composition selection is to add a small amount of the β-stabilizing elements (W and Cr) and the strengthening element boron to the high-Nb TiAl alloy. Band-like segregation bands exist in the lamellar matrix, which are usually found in other high-Nb TiAl alloys. The blocky γ phase generally occurs at the boundary of lamellar colonies and is usually adjacent to the B2 phase and extends along the α_2/γ lamellar direction, as shown in Fig. 2(a). Cheng *et al.* [28] studied the decomposition of the β phase and found that the retained β phase can partially transform to the γ phase by a process analogous to the discontinuous coarsening of γ lamellae. The average size of the lamellar colony from the cross-section of the DS samples was 286 ± 67 μm, which was refined by tuning the DS parameters and adding boron [26]. A small amount of added W and Cr allowed the B2 and adjacent γ phases to be dispersed and not connected in large blocks. From Figs. 2(d), (e), and (f), Nb, W, and Cr are enriched in the B2 phase compared to the blocky γ phase and lamellae.

The results of EDS analysis of the individual phases are summarized in Table 1. The lamellar matrix contains short rod-shaped borides (marked with red arrows in Fig. 2(g)) The statistical results of the phase content show that the volume fractions of the B2 phase, the blocky γ phase and the boride phase are 6.8 ± 0.5%, 8.3 ± 0.7% and 0.4 ± 0.1%, respectively.

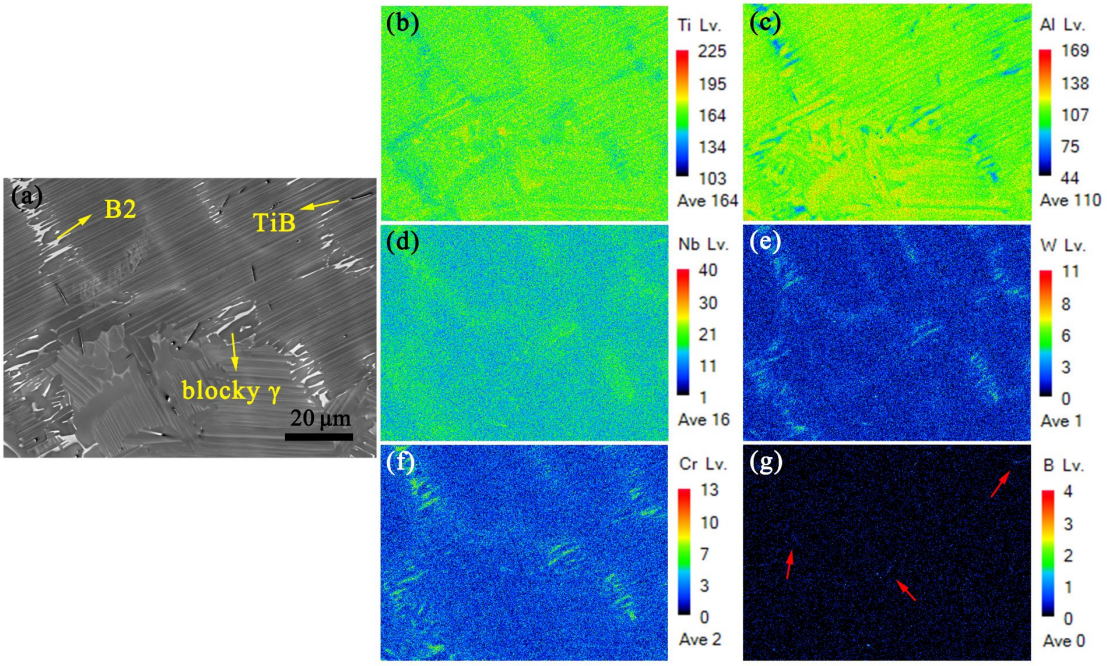

Fig. 2 SEM image and EPMA-WDS mapping results of the Ti46Al7Nb0.4W0.6Cr0.1B alloy. (a) BSE image; (b) Ti; (c) Al; (d) Nb; (e) W; (f) Cr; (g) B.

Table 1 Elemental composition of constitute phases in the Ti46Al7Nb0.4W0.6Cr0.1B alloy derived from EDX

Phase	Composition in at. %				
	Ti	Al	Nb	W	Cr
B2	52.3±0.7	35.9±0.8	8.5±0.2	1.5±0.2	1.8±0.3
Blocky γ	45.3±0.8	46.8±0.6	6.8±0.2	0.5±0.1	0.6±0.1
α_2/γ lamellae	47.5±0.7	44.8±0.7	6.6±0.2	0.4±0.1	0.7±0.1

Fig. 3 shows bright-field and STEM images of the Ti46Al7Nb0.4W0.6Cr0.1B alloy. Figs. 3(b)–(g) show the EDS mapping results. The B2 phase of the alloy is enriched in W and Cr, while the Ti, Nb, W, and B contents in the borides is higher than those in the surrounding regions. Selected area electron diffraction (SAED) analysis

was performed on the boride, B2, and γ phases (marked in yellow, red, and blue, respectively), and the results are shown in Figs. 3(h), (j), and (k), respectively. The SAED results show that the boride phase is a TiB phase with a B27 structure and is enriched in Nb, and W. Liu *et al.* [29] found that TiB with a B27 structure is enriched in both Nb and Ta, but depleted in Mn. Moreover, stacking faults parallel to the (010) plane can be observed in Fig. 3(i).

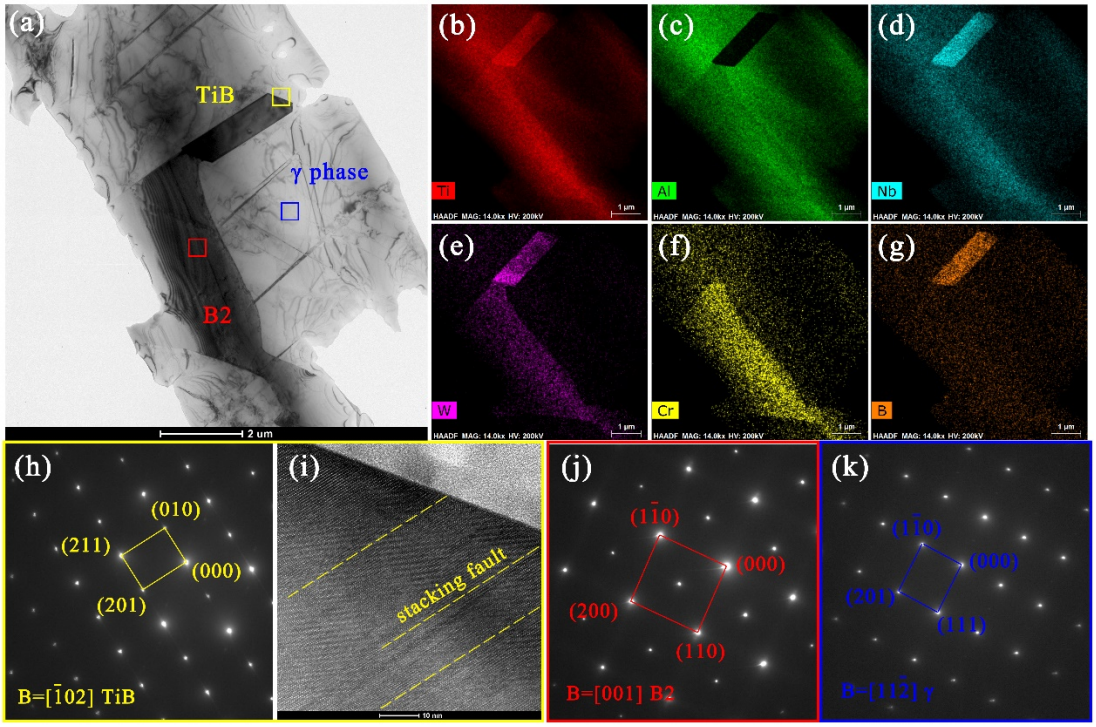

Fig. 3 Bright field (BF) and STEM images of the Ti46Al7Nb0.4W0.6Cr0.1B alloy. (a) BF image; (b) Ti; (c) Al; (d)Nb; (e) W; (f) Cr; (g) B; SAED images of (h) TiB; (j) B2; (k) γ; (i) HRTEM of the TiB phase.

3.2 Rotating bending fatigue properties

Fig. 4 shows the S-N curves of the Ti46Al7Nb0.4W0.6Cr0.1B alloy. The initial fatigue test stress of this experiment was set to 450 MPa and was decreased in steps of 10 MPa to the final test stress amplitude without fracture. The fatigue life reached 10^7 cycles for fatigue test stress values of 400 MPa and below, which is excellent compared to earlier reports [30-32]. Wu *et al.* [30] reported that the rotating-bending fatigue limit of a high Nb TiAl alloy was 355 MPa at 800℃. The fatigue response of TiAl alloys is closely related to the temperature. Some researchers [33] have pointed out that the fatigue growth rate of TiAl alloys at 800℃ is lower than room temperature under air conditions, and it is the lowest around the brittle to ductile transition temperature.

Similar studies at different temperatures can also be found in Refs [16, 34]. Therefore, owing to the characteristics of the TiAl alloy, it has a lower fatigue crack growth resistance at room temperature (25℃), whereas this alloy exhibits a higher fatigue performance. The fatigue deformation of this alloy is analyzed in detail in the following section.

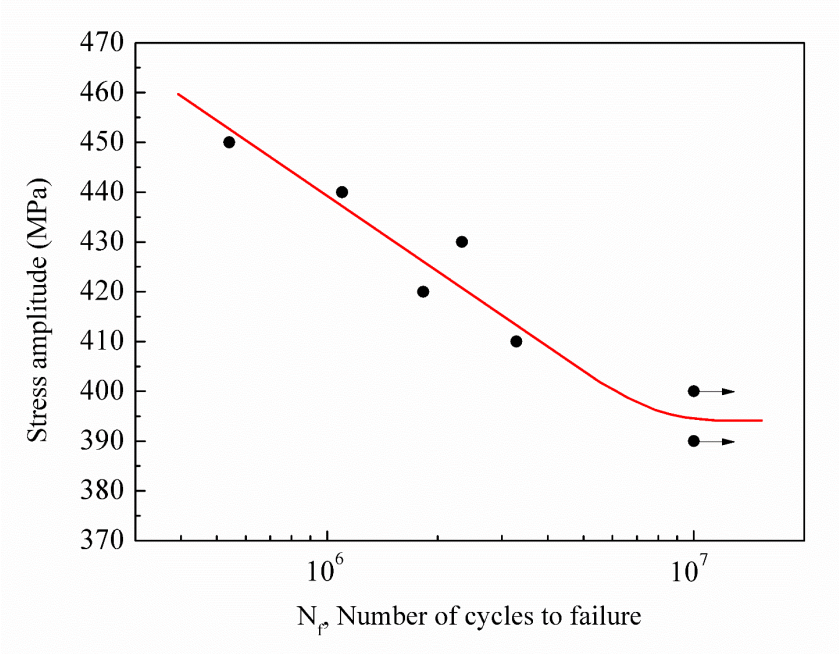

Fig. 4 The S-N curves of the high-cycle rotating bending fatigue the Ti46Al7Nb0.4W0.6Cr0.1B alloy at room temperature

3.3 Deformation behavior of the blocky γ and B2 phase

3.3.1 Deformed microstructure of the blocky γ phase

Fatigue deformation and fracture processes are usually accompanied by the nucleation and propagation of cracks. For TiAl alloys with low room-temperature ductility, once cracks form, fatigue fracture occurs quickly, thereby indicating that crack nucleation plays a crucial role in the fatigue process of TiAl alloys. The study of fatigue deformation behavior can provide an effective basis for revealing nucleation sites and the cause of fatigue crack nucleation. Traditional TiAl alloys are generally composed of the α_2 and γ phases. When the Al content was high, the volume fraction of the γ phase in the lamellar matrix was higher than that of the α_2 phase. The γ phase has a face-centered tetragonal structure, which has more slip systems and is more amenable to deformation than the hexagonal close-packed α_2 phase.

Fig. 5 shows a bright-field TEM image of the deformed structure in the γ phase of

the DS Ti46Al7Nb0.4W0.6Cr0.1B alloy specimen after fatigue testing at room temperature. There were many dislocations in the γ phase, and the dislocation density in the γ phase was higher than that at the boundary of the γ and B2 phases. Figs. 5(a), (b), and (c) show the TEM images of the γ phase at g = [002], [111], and [110], respectively. Figs. 5(d), (e), and (f) show enlarged images of the middle position in the image above. When g = [002] and [110], the number of visible dislocations in the γ phase was greater, and when g = [111], the number of visible dislocations was lower. According to the $\boldsymbol{g}\cdot\boldsymbol{b}$ criterion, the Burgers vector for most dislocations was $[01\bar{1}]$. The twin structures at the lamellar boundaries were aligned parallel to each other. In the initial stage of twinning nucleation, the Shockley partial dislocation with 1/6<112] Burgers vector slips on the (111) plane, which generates a superlattice intrinsic stacking fault (SISF) [35]. In addition to parallel-aligned twins, twin intersections exist in the γ phase after fatigue deformation. Twin intersections in TiAl alloys can be observed under different stress states such as high-temperature creep [36], hot compression [37] and room-temperature compression [38]. Twins and twin intersections can reduce the dislocation mean free path by introducing extra interfaces [39,40], thus resulting in a significantly enhanced strain-hardening effect and strengthening of the alloy matrix. Therefore, the deformation of the γ phase in this alloy was mainly composed of superlattice dislocation movement and twinning deformation. Abundant deformation modes are of great significance to the fatigue properties of high-Nb TiAl alloys, with the γ phase as the main deformation phase.

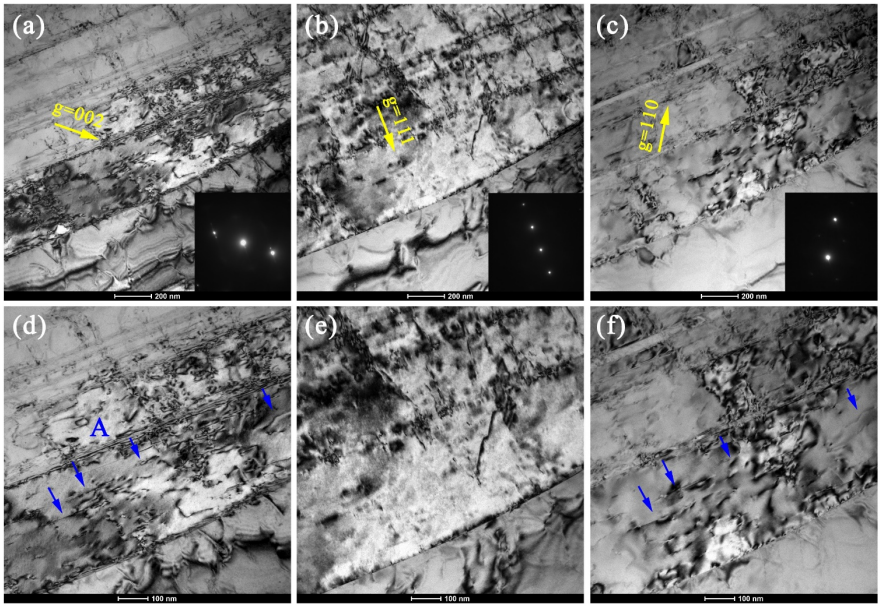

Fig. 5 TEM micrographs of the deformed γ phase region in the high-Nb TiAl alloy after high-cycle fatigue test. (a) g=(002); (b) g=(111); (c) g=(110); (d), (e), and (f) are the

enlarged images of (a), (b), and (c), respectively.

3.3.2 Deformed microstructure of the B2 phase

Fig. 6 shows a bright-field TEM image of the deformed structure in the B2 phase of the DS Ti46Al7Nb0.4W0.6Cr0.1B alloy specimen after fatigue testing at room temperature. The region surrounded by the green dotted line represents the B2 phase, and the upper and lower sides correspond to the γ phase. The dislocation density in the B2 phase was very high, but no twins were observed. The existence of high-density dislocations in the B2 phase indicates that the deformation mode of the B2 phase at room temperature was dominated by dislocation slip and exhibits good room-temperature deformability. Figs. 6(a), (b), (c), and (d) show the TEM images of the B2 phase at g = [011], [$\bar{1}\bar{1}\bar{1}$], [100], and [$\bar{1}$00], respectively. Figs. 6(e), (f), (g), and (h) show enlarged images of the central area of the above image, respectively. When g = [011], [100], or [$\bar{1}$00], a large number of dislocations were found inside the B2 phase. The dislocations distributed in the B2 phase were short and scattered, and the dislocations close to the phase boundary were tangled and mostly parallel to the boundary. When g = [$\bar{1}\bar{1}\bar{1}$], no dislocations were observed inside or at the boundary of the B2 phase. For the two opposite directions [100] and [$\bar{1}$00], the number and distribution of dislocations remain the same, but the contrast between the left and right images is symmetrical because of the difference in the viewing direction and bending of the specimen, as shown in Figs. 6(g) and (h). A-type dislocations are visible with g = [011], [100], and [$\bar{1}$00], but invisible with g = [$\bar{1}\bar{1}\bar{1}$], as shown by the blue arrows in Figs. 6(e) and (g). Therefore, the main deformation mode of the B2 phase is a dislocation slip with a Burgers vector <110>. In addition, a small number of B-type dislocations are visible with g = [100], [$\bar{1}$00], [$\bar{1}\bar{1}\bar{1}$], but invisible with g = [011], as indicated by the red arrows in Figs. 6(f) and (g). Hence, there are still a few dislocations that slip with Burger vectors [100] and [11$\bar{1}$].

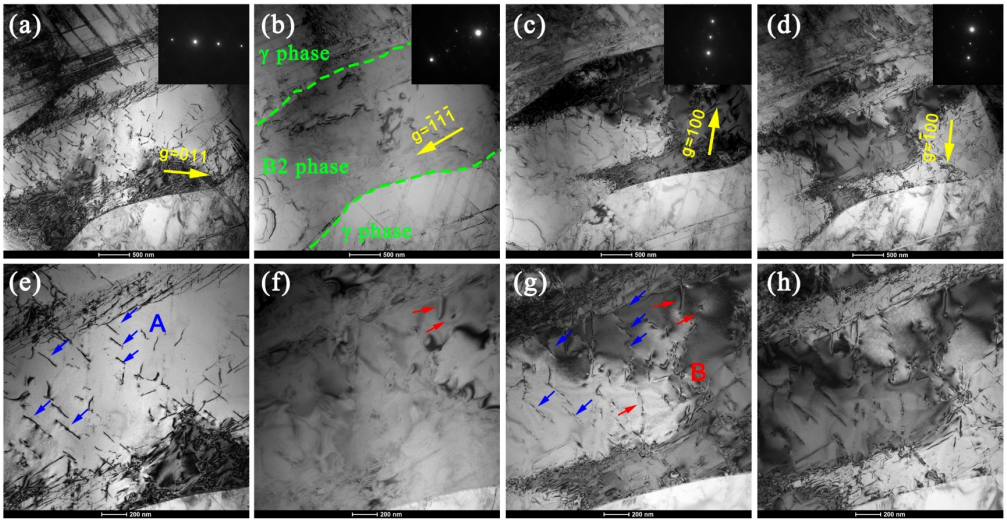

Fig. 6 TEM micrographs of the deformed B2 phase region in the high-Nb TiAl alloy after high-cycle fatigue test. (a) g=(011); (b) g=($\bar{1}\bar{1}\bar{1}$); (c) g=(100); (d) g=($\bar{1}$11); (e), (f), (g), and (h) are the enlarged images of (a), (b), (c), and (d), respectively.

The B2 phase is a long-range ordered body-center-cubic (bcc) phase with mixed metallic and covalent bonding. Usually, the B2 phase lacks sufficient slip systems and cannot satisfy the Von Mises condition because of the high anti-phase boundary (APB) energy, and this results in its poor ductility at room temperature [41]. The B2 phase exists in many alloys, including NiAl, CoTi, YAg, and DyCu, which exhibit various brittle or plastic characteristics owing to their different slip systems. Mulay *et al.* [42] found that <100>{011} and <100>{001} slip systems in CoTi alloys can be activated under low stress. Dislocation slip with <110> and <111> Burger vectors under high stress conditions can effectively reduce stress concentration and thus avoid premature failure. Russell *et al.* [43] found that the main deformation of the YAg alloy was <111> type dislocations with some <011> dislocations. Xing *et al.* [44] studied the deformation behavior of NiAl alloys by means of first-principles calculations and found that the stacking fault energy of <001> is higher than that of <111>, but a high APB prevents the nucleation of <111> dislocations, which leads to room-temperature brittleness of the alloy. The deformation of NiAl alloys at low temperatures is mainly <111> {112} slip. Cao *et al.* [45] found that <001> and <111> slip were the main deformation modes in DyCu, and slip in the <111> direction satisfied the von Mises criterion and explained its high plasticity and fracture toughness.

According to the Von Mises criterion, the crystal must have five independent slip systems to obtain uniform strain conditions and thus have better plastic deformability.

Some studies [46,47] have indicated that only the following four groups of slip modes have five independent slip systems in the B2 crystal structure: (1)<111>{011}, (2)<111>{112}, (3)<110 >{111}, and (4)<100>{011}+<011>{011}. As for the deformation mode of the B2 phase in the TiAl alloy, Yang *et al.* [48] conducted rotating bending fatigue tests on a high-Nb TiAl alloy at high temperatures and showed that the deformation mechanism of the B2 phase may be dislocation glide with the <111> Burgers vector. Similar studies focusing on the same Burgers vector can be found in Ref [24]. However, the <110>- and <001>-type dislocations of the B2 phase can also be activated when the samples are deformed at different temperatures [25]. The above research shows that the Burgers vectors <001>, <110>, and <111>-type dislocations appear in the B2 phase of TiAl alloys. The main deformation mode of the B2 phase in this study is the dislocations with the <110> type Burgers vector, which indicates that the B2 phase can undergo substantial plastic deformation.

From the perspective of chemical composition, the B2 phase in this alloy is enriched with Cr, as shown in Table 1 and Figs. 2 and 3. Although only 0.6% Cr was added to ensure that no excess B2 phase was introduced into the alloy matrix, the EDS results indicate that the content of Cr in the B2 phase was 1.8%, which is three times the nominal content. The β-stabilizing ability of Cr is stronger than that of elements such as Nb and V and weaker than that of Fe, W, and Mo, and Cr can easily segregate in the B2 phase [10]. Kartavykh *et al.* [49] pointed out that the accumulation of Cr in the B2 phase can enhance the ductility of β-stabilized TiAl alloys. They attributed the good RT tensile deformability of the alloy to the softening of the Cr-alloyed B2 intergranular phase by the mutually exclusive redistribution of Cr and Zr between the conjugate γ and B2 phases. Liu *et al.* [50] also found that the B2 phase of V and Cr additions is beneficial for the room temperature ductility. Our previous study [51] also showed that an increase in Cr content decreases the nanohardness of the B2 phase owing to the tendency to reduce lattice distortion. Therefore, Cr microalloying can promote the deformability of the B2 phase in high-Nb TiAl alloys without an excessive volume fraction of the large bulk B2 phases. This is helpful in mitigating incompatibility with the deformation of the surrounding matrix owing to the existence of the hard B2 phase. This result also explains the good fatigue properties of the high-Nb microalloyed TiAl alloy.

3.4 Coordinated deformation behavior between the B2 and blocky γ phase

3.4.1 TEM observation at the interface of B2 and blocky γ phase

Fig. 7 shows TEM images of the different phases in DS Ti46Al7Nb0.4W0.6Cr0.1B after fatigue deformation. In multiphase TiAl alloys, each phase exhibits different deformation modes. The deformation was mainly concentrated in the B2 and γ phases, and there was almost no deformation in the α_2 phase, as shown in Fig. 7(a). A large number of dislocations gathered near the interface between the B2 and γ phases, indicating that the phase interface could effectively hinder the continuous movement of dislocations. The dislocation density at the interface was significantly higher than that inside the B2 phase. On the γ-phase side, the twins terminated at the interface of the B2 and γ phases. On the B2 phase side of the twin-terminated interface, there were usually more dislocations than at other locations on the interface, as indicated by the yellow arrows in Fig. 7(b). This indicates that twinning on the γ-phase side had a significant effect on the dislocations on the B2 phase side. In particular, the dislocation density on both sides is high at the twin intersection in the γ phase near the boundary, which indicates that the twin intersection seriously hindered the movement of dislocations and caused dislocations to be blocked in the locally strained region. Many dislocations from the B2 phase side indicated that the strain region generated by the twin intersections of the γ phase promoted the initiation and propagation of dislocations in the B2 phase. This result was also confirmed at the position indicated by the yellow arrow in the upper part of Fig. 7(b).

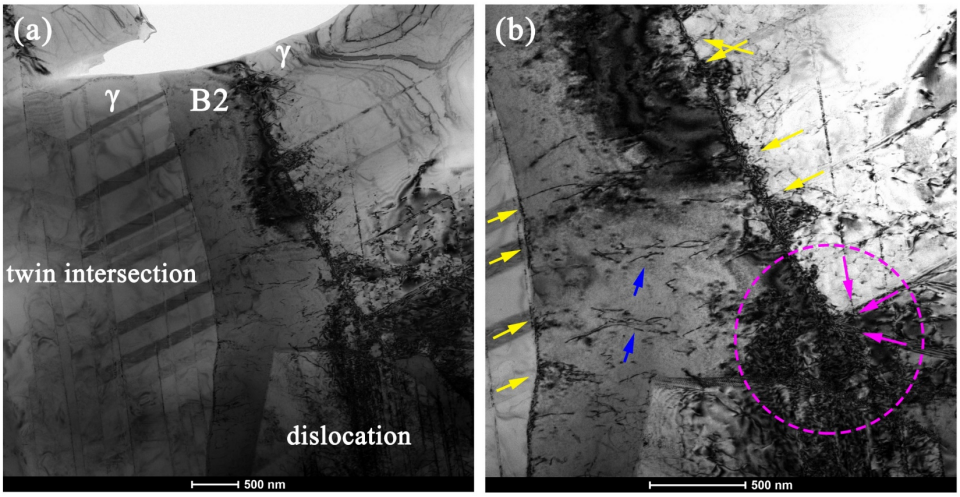

Fig. 7 TEM observation of deformed microstructure in the high-Nb TiAl alloy after high-cycle fatigue test. (a) Deformation transfer between B2 and γ phases; (b) Magnified image of a.

Fig. 8 shows the deformed microstructure near the B2 and blocky γ phases. Fig. 8(b) shows an enlarged image of the red dashed box in (a). Deformation twins interlaced

with each other appear in the γ phase (blue arrows in Fig. 8(a)), and many dislocations appear in the B2 phase (red arrows in Fig. 8(b)). This phenomenon indicated that deformation in the B2 phase was dominated by dislocation movement and the deformation in the γ phase was dominated by twinning and dislocation movement. The γ phase deformed easily, whereas the B2 phase is difficult to deform at room temperature [52,53]. However, this study shows that the B2 phase can also deform to a certain extent through dislocation nucleation and multiplication, which could be an important reason for the excellent rotating-bending fatigue properties of the alloy. A very interesting effect can be observed more clearly in Fig. 8(b). The deformation twins in the γ phase terminated at the interface between the B2 and γ phases, and there was evidence of dislocation nucleation and multiplication on the B2 side of the interface. This phenomenon is clearly observed in the two yellow dashed circles in Fig. 8(b). This explains why the B2 phase can deform at room temperature. In addition, dislocations in the B2 phase are formed by the activation of deformation twins in the adjacent γ phase.

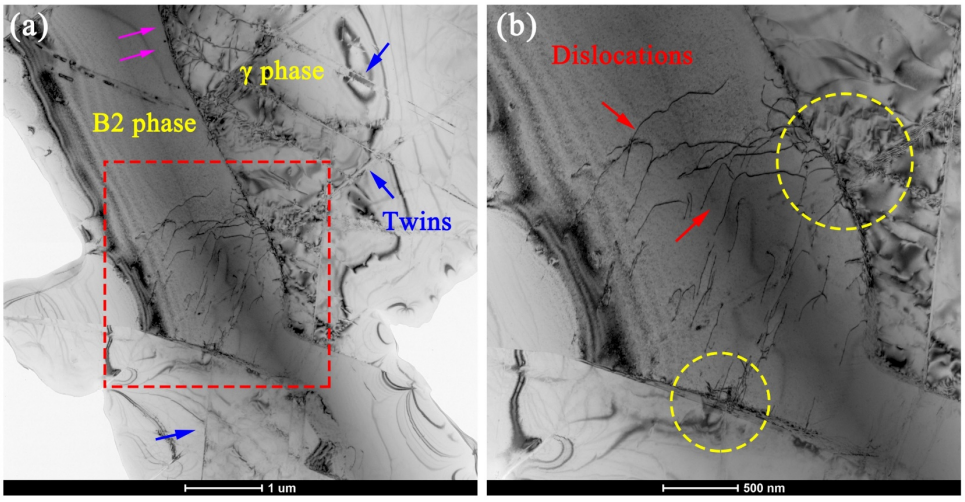

Fig. 8 TEM images of the high-Nb TiAl alloy after high-cycle fatigue test. (a) Twins in blocky γ induce the formation of dislocations in B2 phases; (b) Magnified image of the red dashed box in b.

For multiphase materials, the deformation between the soft phase and the hard phase first appears in the soft phase, and as the degree of deformation increases, the soft phase undergoes work hardening, and then the hard phase begins to deform. In studying the stress transfer and dislocation nucleation processes of DS multiphase ordered Ni-Fe-Al alloys, Misra *et al.* [54] found that at very low strains, dislocation slip occurs

only in the softer γ phase near the interface. This result is consistent with the observation in other DS eutectic Ni(fcc)-W(bcc) alloys, where the initiation of dislocation slip occurs in the softer Ni phase [55]. The B2 phase in multiphase TiAl alloys is usually harder than the γ phase [5,56]. Therefore, the slip of the γ phase will first be activated during the fatigue test. It is difficult for the chemically ordered B2 phase to be deformed owing to the insufficient slip systems and APB energy, and the interconnected bulk B2 phase can seriously impair the properties. There will be considerable dislocation blocking and stress concentration at the interface between the hard B2 phase and the soft γ phase. When the stress concentration cannot be relieved or accommodated by the continuous slip and other deformation modes, cracks occur at the interface or within the B2 phase, thereby causing material failure. This results in poor mechanical properties of TiAl alloys containing a large amount of the B2 phase. However, if the B2 phase is dispersed in the form of small precipitates, it provides a precipitation-strengthening effect.

Some researchers [57,58] studied the creep properties of a TiAl alloy with W addition and found that interfacial β-precipitates reduced the instantaneous strain and improved the rupture life. Because the B2/γ interface is usually semi-coherent, misfit dislocations or interfacial dislocations are generated at the interface to reduce the elastic strain energy of the interface. Defects, such as misfit dislocations at these interfaces, can often act as heterogeneous nucleation sites for twinning [35,59]. Furthermore, high Nb content can reduce the stacking fault energy of the γ phase, resulting in the generation of stacking faults in the γ phase [60]. The stacking fault energy is closely related to the atomic bonding strength; Nb addition can locally decrease the degree of covalent bonding, which can result in a decrease in the stacking fault energy [61]. Under the action of continuous stress, stacking faults gradually evolve into twins; hence, twinned structures are usually be observed in the γ phase of deformed high-Nb TiAl alloys. It is usually difficult for fcc-based crystal twinning to occur; however, owing to the presence of misfit dislocations and low stacking fault energy, twins can appear in the γ phase during fatigue deformation. Dislocations can also be observed in the γ phase, and are widely distributed inside the γ phase and intersect with twins. This indicates that the deformation of the γ phase is dominated by both dislocations and twins, reflecting its softness and good deformability. Under stress, the γ phase undergoes a strain-hardening effect owing to abundant dislocation slip and twinning. This increases the flow stress of the γ phase to continuous deformation and results in a local strain zone at the phase interface. The strain hardening of the softer γ phase activates the

deformation of the adjacent hard B2 phase with dislocation slip because the interface is a local strain accumulation region. This means that the local stresses at the phase interface were accommodated by the deformation twins, twin intersections of the γ phase, and by the continuous dislocation slip in the B2 phase.

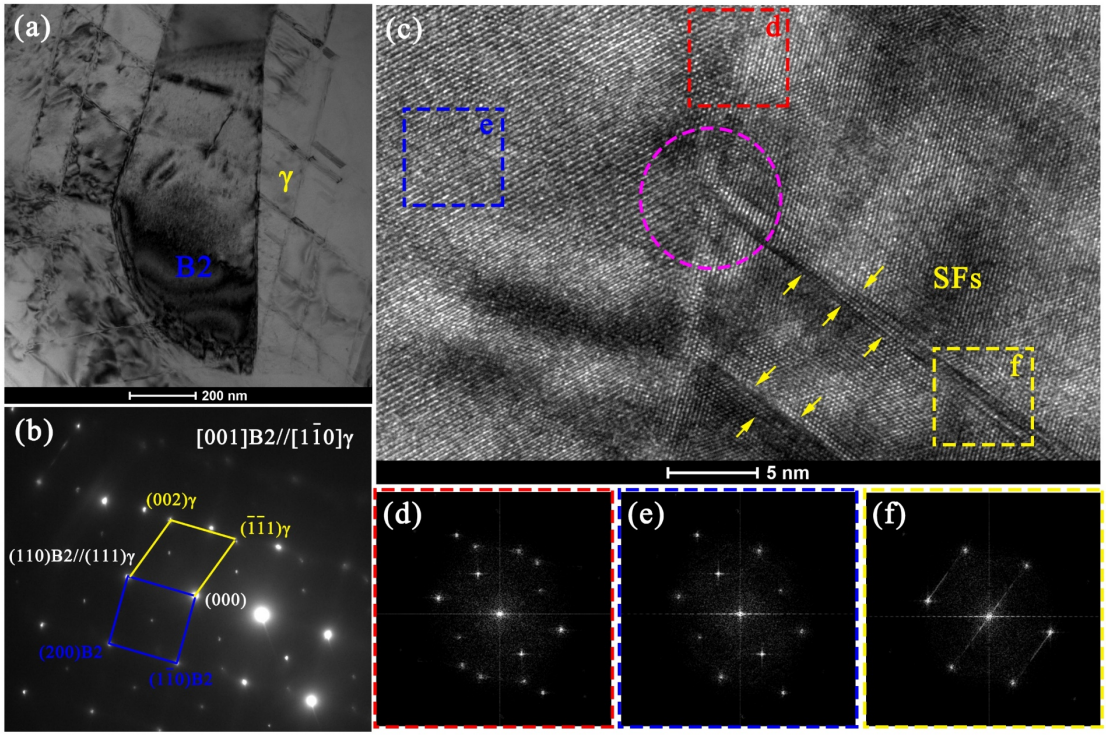

Fig. 9 TEM observation at the interface of B2 and γ phase in the high-Nb TiAl alloy after high-cycle fatigue deformation. (a) BF image; (b) SAED of B2 and γ; (c) HRTEM of the interface; (d), (e) and (f) are the FFT of red, blue and pink box, respectively.

Fig. 9 shows the TEM images at the interface between the B2 and γ phases after fatigue deformation. Fig. 9(a) shows a bright-field image. SAED and HRTEM observations were noted at the interface and the results are presented in Figs. 9(b) and (c), respectively. The diffraction pattern reveals that the B2 and γ phases satisfied the orientation relationship of (110)B2//(111)γ and [001]B2//[1$\bar{1}$0]γ. Fast Fourier transform (FFT) was performed on the blue, red, and yellow regions in Fig. 9(c), and the images are shown in Figs. 9(d), (e), and (f), respectively. The blue area is the B2 phase, the red area is the interface of the B2 and γ phases, and the yellow area is the γ phase. The interface of the face-centered cubic (fcc)-based and body-centered cubic (bcc)-based B2 phases is predominantly determined by the Kurdjumov-Sachs (K-S) and Nishiyama-Wasserman (N-W) orientation relationships [62]. The incommensurate interfaces

formed by such orientation relationships are usually semi-coherent, flat, free of steps, and contain misfit dislocations with in-plane Burgers vectors [63]. Overall, the role of interfaces during the plastic deformation of metals is as follows: (i) nucleation sites of defects, (ii) absorption and annihilation sites of defects, and (iii) barriers to the transmission of defects. The slip transmission across the interface depends on the shear resistance of the interface, and the fcc/bcc interface has a high resistance to dislocation slip transfer [64]. Therefore, simply trying to slip across the phase interface by dislocations is difficult. Stacking faults parallel to the (111) plane can be observed, which can also be verified by the broadened streaking along the spots in Fig. 9(f). The stacking fault in the γ phase ends at the interface between the γ and B2 phases, and cannot pass through the phase interface. Strain regions were generated at the interface, and the arrangement of atoms in the strain region was relatively disordered. The pink dotted circle in Fig. 9(c) shows that there is a disordered region on the side of the B2 phase at the intersection of the interface and the stacking faults; dislocations with the Burgers vector <110> can be observed. The twins in the γ phase changed the atomic arrangement of the locally strained region near the interface. Once the B2 phase dislocation slip condition is satisfied, dislocations will initiate and continue to propagate in the B2 phase, which will release the stress concentration at the phase interface and realize stress transfer between these two phases.

3.4.2 Mechanism of the dislocations in bcc-based phase induced by twins in fcc-based phase

Liu *et al.* [50] studied the tensile deformation behavior of triplex TiAl alloys, and the possible deformation modes of the constituent phases in TiAl were preliminarily discussed. Co-deformation behavior between bcc-based and fcc-based phases exists in many alloys. A previous study [65] provided details on the investigation of the B2 phase to enhance the mechanical properties of fcc-based high-entropy alloys and revealed that the B2 phase can promote twinning of the fcc phase by increasing the local stress level. The underlying role of the harder B2 phase in promoting deformation twins in neighboring fcc grains was determined using molecular dynamic simulations and TEM observations. This study provides more direct evidence that the <110>-type dislocation slip in the B2 phase can be activated by the twinning of the γ phase, thereby promoting stress transfer and obtaining excellent fatigue properties.

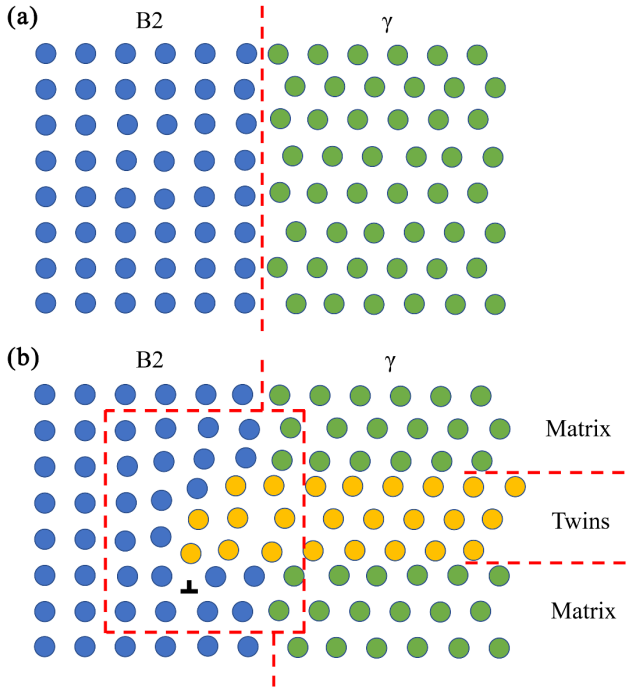

Fig. 10 Schematic diagram of dislocation formation in B2 phase induced by twins in adjacent γ phase. (a) Origin atomic arrangement at the interface of B2 and γ; (b) Dislocation induced by twins

Fig. 10 shows a schematic diagram of dislocation formation in the B2 phase induced by twins in the adjacent γ phase. First, at the phase interface, although there is an orientation relationship between the B2 and γ phases, the difference in crystal structure results in a semi-coherent interface; hence, there are interfacial dislocations at the phase interface to absorb this mismatch. According to previous results of dislocations in the γ phase (Fig. 5), the $[01\bar{1}]$ Burgers vector dislocation slip is dominant in the γ phase, which is a typical superlattice dislocation in the γ phase. It generates a Shockley partial dislocation, Frank partial dislocation, and SISF through the dissociation of an ordinary dislocation by the reaction [66]

$$1/2[110] = 1/3[111] + \text{SISF} + 1/6[11\bar{1}]$$

The uniform shear of the deformed twins is completed by the slip of the Shockley partial dislocations, which causes each atomic plane of the deformed twins to produce the same displacement relative to the adjacent atomic plane along the twinning direction. When a twin structure is formed, it has a significant effect on the atomic arrangement at the interface. The local atomic arrangement was altered from a slip-resistant orientation to a slip-friendly orientation, which aided the dislocation slip of the <110> Burgers vector of the B2 phase (Fig. 10(b)). Choudhuri *et al.* [67] studied the

deformation of fcc-B2 nanostructures containing a K-S interface and showed that the interaction between this interface and $\{111\}_{fcc}$ stacking faults can activate a $<111>_{B2}$ dislocation on the $\{110\}_{B2}$ plane. Gao *et al.* [68] found that the occurrence of a back-stress effect could result in the interaction of dislocations in the $L1_2$ phase with the phase interface, and activate more dislocations on the {110} plane in the B2 phase. In this study, the interaction of the stacking faults along the {111} plane in the γ phase and phase interface activates a <110> type dislocation in the adjacent B2 phase.

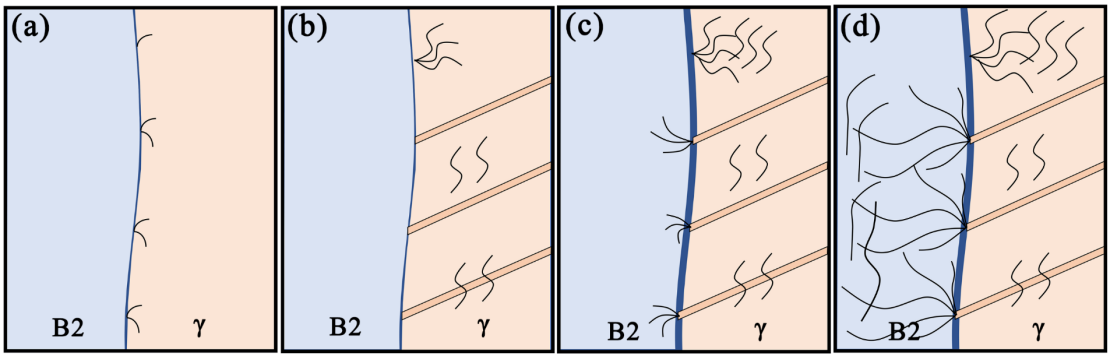

Fig. 11 Schematic diagram of twin inducing dislocations process. (a) Misfit dislocations at the interface of the γ and the B2 phases; (b) Twins generated and intersect with dislocations; (c) Twins in the γ phase induce dislocation nucleation on the B2 side of the interface; (d) Dislocation multiplication in the B2 phase.

During the fatigue deformation process, the coordinated deformation process between the B2 and γ phases in the microalloyed high-Nb TiAl alloy can be summarized as follows: First, a small amount of a β-stabilizing element was added to the high-Nb TiAl alloy produced by a directional solidification process. Coupling of the B2 and γ phases dispersed at the boundary of the lamellar colonies was obtained. Owing to the high Nb content, the low stacking fault energy of the γ phase and semi-coherent relationship with the B2 phase led to the formation of partial dislocations at the phase interface (Fig. 11(a)) and the generation of stacking faults in the γ phase. The stacking fault slips along the (111) plane to form a parallel twin structure (Fig. 11(b)). The twins present at the interface change the crystallographic orientation around the interface, which can result in the transformation of an orientation that is unfavorable for slip to an orientation that is favorable for slip. This effect promotes further slip and crystal deformation, to induce dislocation nucleation on the B2 phase side of the interface (Fig. 11(c)). After the dislocations nucleate, the dislocations in the B2 phase slip and multiply along the corresponding slip planes (Fig. 11(d)), thus resulting in a stress transfer

between the γ and B2 phases. Effective stress transfer and deformation between two adjacent phases can only be achieved by providing the other phase with a suitable orientation for slip through atomic rearrangement of the interface by twinning.

4. Conclusions

In summary, high-cycle rotating bending fatigue tests were carried out on a microalloyed high-Nb TiAl alloy at room temperature, and a coordinated deformation mechanism was revealed by TEM analysis. The main conclusions can be summarized as follows,

(1) The high-Nb TiAl alloy has a predominantly lamellar microstructure, as well as a coupled structure formed by the B2 phase, blocky γ phase dispersed between and inside the lamellar colonies, and the TiB phase embedded in the lamellae. These are responsible for enhancing the fatigue resistance. The high-Nb TiAl alloy underwent 10^7 cycles of rotating-bending fatigue test under a stress amplitude of 400MPa without fracture.

(2) Through TEM diffraction analysis, the fatigue deformation in the γ phase was dominated by superlattice dislocations $[01\bar{1}]$ and twinning at room temperature, and the deformation in the B2 phase was dominated by <110> Burgers vector dislocations.

(3) The addition of a large amount of Nb reduced the stacking fault energy of the γ phase, which promoted the twinning in the γ phase. Stress transfer between the two adjacent B2 and γ phases occurred through the atomic rearrangement of the interface by twinning.

(4) The good room-temperature rotating bending fatigue properties of this alloy can be attributed to dispersion strengthening by the TiB phase and dislocation slip in the B2 phase induced by twins formed in the adjacent γ phase. This resulted in effective stress transfer and coordinated deformation during high-cycle fatigue.

Acknowledgement

The authors would like to acknowledge the financial support from the National Natural Science Foundation of China under Grant Nos. 52171112. This work is supported by AME Programmatic Fund by the Agency for Science, Technology and Research, Singapore under Grant No A18B1b0061. X. Xu acknowledges the fellowship from China Scholarship Council.

References

[1] G. Zheng, B. Tang, S. Zhao, W.Y. Wang, X. Chen, L. Zhu, J. Li, Evading the strength-ductility trade-off at room temperature and achieving ultrahigh plasticity at 800℃ in a TiAl alloy, Acta Mater. 225 (2022) 117585.

[2] R. Gao, H. Peng, H. Guo, B. Chen, An innovative way to fabricate γ-TiAl blades and their failure mechanisms under thermal shock, Scripta Mater. 203 (2021) 114092.

[3] B.P. Bewlay, S. Nag, A. Suzuki, M. J. Weimer, TiAl alloys in commercial aircraft engines, Mater High Temp. 33 (2016) 549-559.

[4] H. Clemens, S. Mayer, Design, Processing, Microstructure, Properties, and Applications of Advanced Intermetallic TiAl Alloys Adv. Eng. Mater. 15 (2013) 191-215.

[5] M. Schloffer, B. Rashkova, T. Schöberl, E. Schwaighofer, Z. Zhang, H. Clemens, S. Mayer, Evolution of the ω_o phase in a β-stabilized multi-phase TiAl alloy and its effect on hardness, Acta Mater. 64 (2014) 241-252.

[6] G. Chen, Y.B. Peng, G. Zheng, Z.X. Qi, M.Z. Wang, H.C. Yu, C.L. Dong, C.T. Liu, Polysynthetic twinned TiAl single crystals for high-temperature applications, Nat. Mater. 15 (2016) 876-881.

[7] W.J. Zhang, S.C. Deevi, G.L. Chen, On the origin of superior high strength of Ti–45Al–10Nb alloys, Intermetallics 10 (2002) 403-406.

[8] Leitner T, Schloffer M, Mayer S, Eßlinger J, Clemens H, Pippan R. Fracture and R-curve behavior of an intermetallic β-stabilized TiAl alloy with different nearly lamellar microstructures, Intermetallics, 2014, 53,1-9.

[9] B. Zhu, X. Xue, H. Kou, X. Li, J. Li, The cavitation of high Nb-containing TiAl alloys during tensile tests around BDTT, Mater. Sci. Eng. A 729 (2018) 86-93.

[10] F. Sun, C. Cao, S. Kim, Y. Lee, M. Yan, Alloying Mechanism of Beta Stabilizers in a TiAl Alloy, Metall. Mater Trans A 32 (1997) 1573-1589.

[11] Z. Wu, R. Hu, T. Zhang, H. Zhou, H. Kou, J. Li, Microstructure determined fracture behavior of a high Nb containing TiAl alloy, Mater. Sci. Eng. A 666 (2016) 297-304.

[12] J.P. Campbell, K.T. Venkateswara Rao, R.O. Ritchie, On the role of microstructure in fatigue-crack growth of γ-based titanium aluminides, Mater. Sci. Eng. A 239–240 (1997) 722–728.

[13] M.S. Dahar, S.A. Tamirisakandala, J.J. Lewandowski, Evolution of fatigue crack growth and fracture behavior in gamma titanium aluminide Ti-43.5Al-4Nb-1Mo-0.1B (TNM) forgings, Int. J. Fatigue, 111 (2018) 54–69.

[14] M.S. Dahar, S.A. Tamirisakandala, J.J. Lewandowski, Fatigue crack growth and fracture behavior of as-cast Ti-43.5Al-4Nb-1Mo- 0.1B (TNM) compared to Ti-48Al-2Nb-2Cr (4822), Intermetallics 91 (2017) 158–168.

[15] L.J. Signori, T. Nakamura, Y. Okada, R. Yamagata, H. Nakashima, M. Takeyama, Fatigue crack growth behavior of wrought γ-based TiAl alloy containing β-phase,

Intermetallics 100 (2018) 77–87.
[16] M. Sakaguchi, Y. Niwa, W. Gong, K. Suzuki, H. Inoue, Temperature dependent fatigue crack growth in forged TiAl alloys with nearly-lamellar and triplex microstructure, Mater. Sci. Eng. A 806 (2021) 140802.
[17] C. Dong, H. Yu, Z. Jiao, F. Kong, Y. Chen, Low cycle fatigue, creep and creep-fatigue interaction behavior of a TiAl alloy at high temperatures, Scripta Mater. 144 (2018) 60-63.
[18] X. Gu, S. Jiang, F. Cao, G. Zhang, D. Yang, S. Guo, H. Song, J. Sun, A β-solidifying TiAl alloy reinforced with ultra-fine Y-rich precipitates, Scripta Mater. 192 (2021) 55-60.
[19] A. Couret, J. Monchoux, D. Caillard, On the high creep strength of the W containing IRIS-TiAl alloy at 850°C, Acta Mater. 181 (2019) 331-341.
[20] B. Selvarajou, M.H. Jhon, R.V. Ramanujan, S.S. Quek, Temperature dependent anisotropic mechanical behavior of TiAl based alloys, Int. J. Plasticity. 152 (2022) 103175.
[21] R. Hoppe, F. Appel, Deformation-induced internal stresses in multiphase titanium aluminide alloys, Acta Mater. 64 (2014) 169-178.
[22] T.E.J. Edwards, F. D. Gioacchino, A.J. Goodfellow, G. Mohanty, J. Wehrs, J. Michler, W.J. Clegg, Transverse deformation of a lamellar TiAl alloy at high temperature by in situ microcompression, Acta Mater. 166 (2019) 85-99.
[23] L. Song, F. Appel, L. Wang, M. Oehring, X. Hu, A. Stark, J. He, U. Lorenz, T. Zhang, J. Lin, F. Pyczak, New insights into high-temperature deformation and phase transformation mechanisms of lamellar structures in high Nb-containing TiAl alloys, Acta Mater. 186 (2020) 575-586.
[24] M. Kolb, J.M. Wheeler, H.N. Mathur, S. Neumeier, S. Korte-Kerzel, F. Pyczak, J. Michler, M. Göken, Local mechanical properties of the (β0+ω0) composite in multiphase titanium aluminides studied with nanoindentation at room and high temperatures, Mater. Sci. Eng. A 665 (2016)135–140.
[25] H. Liu, Z. Li, F. Gao, Q. Wang, Dislocation structures of B2 phase in Ti-42Al-6V-1Cr alloy deformed at room temperature and 800℃, J. Alloy Compd. 785 (2019) 131-135.
[26] X. Xu, H. Ding, H. Huang, H. Liang, R. Chen, J. Guo, H. Fu, Microstructure formation and columnar to equiaxed transition during cold crucible directional solidification of a high-Nb TiAl alloy, J. Mater. Res. Technol. 11 (2021) 2221-2234.
[27] B. Fultz, J. Howe, Transmission Electron Microscopy and Diffractometry of Materials, third ed., Springer, New York, 2007.
[28] T.T. Cheng, M.H. Loretto, The decomposition of the beta phase in Ti-44Al-8Nb and Ti-44Al-4Nb-4Zr-0.2Si alloys, Acta Mater. 46 (1998) 4801-4819.
[29] B.G. Liu, L.H. Liu, W.D. Xing, R.C. Liu, R. Yang, P.A. Withey, J. Zhu, R. Yu, Structural stability and the alloying effect of TiB polymorphs in TiAl alloys, Intermetallics 90 (2017) 97–102.

[30] Y. Wu, R. Hu, J. Yang, X. Xue, High-temperature rotary-bending fatigue characteristics of a high Nb containing beta-gamma TiAl alloy, Mater. Sci. Eng. A 735 (2018) 40-48.
[31] R. Shrestha, J. Simsiriwong, N. Shamsaei, Fatigue behavior of additive manufactured 316L stainless steel under axial versus rotating-bending loading: Synergistic effects of stress gradient, surface roughness, and volumetric defects, Int. J. Fatigue, 144 (2021) 106063.
[32] G. Nicoletto, Smooth and notch fatigue behavior of selectively laser melted Inconel 718 with as-built surfaces, Int. J. Fatigue, 128 (2019) 105211.
[33] Stephen J. Balsone, James M. Larsen, David C. Maxwell, J. Wayne Jones, Effects of microstructure and temperature on fatigue crack growth in the TiAl alloy Ti-46.5A1-3Nb-2Cr-0.2W, Mater. Sci. Eng. A 192/193 (1995) 457-464.
[34] S.J. Zhu, L.M. Peng, T. Moriya, Y. Mutoh, Effect of stress ratio on fatigue crack growth in TiAl intermetallics at room and elevated temperatures, Mater. Sci. Eng. A 290 (2000) 198–206.
[35] J.W. Christian, S. Mahajan, Deformation twinning, Prog. Mater. Sci. 39 (1995) 1–157.
[36] X. Xu, H. Ding, H. Huang, H. Liang, H. Guo, R. Chen, J. Guo, H. Fu, Twin and twin intersection phenomena in a creep deformed microalloyed directionally solidified high Nb containing TiAl alloy, J. Mater. Sci. Technol. 127 (2022) 115–123.
[37] R. Xu, M. Li, Twinning and twin intersections in γ grains of Ti-42.9Al-4.6Nb-2Cr, J. Mater. Sci. Technol. 88 (2021) 90–98.
[38] J.X. Zhang, H.Q. Ye, Twin intersection in a deformed TiAl alloy, Scripta Mater. 45 (2001) 133-138.
[39] G.L. Chen, L.C. Zhang, TEM investigation of twin intersection in a Ti-45Al-9Nb-2.5Mn alloy deformed at room temperature, Intermetallics 8 (2000) 539-544.
[40] K. Lu, L. Lu, S. Suresh, Strengthening Materials by Engineering Coherent Internal Boundaries at the Nanoscale, Science 324 (2009) 349–352.
[41] F. Appel, J.D.H. Paul, M. Oehring, Gamma titanium aluminide alloys: Science and technology, Wiley-VCH, 2011.
[42] R.P. Mulay, S.R. Agnew, Hard slip mechanisms in B2 CoTi, Acta Mater. 60 (2012) 1784–1794.
[43] A.M. Russell, Z. Zhang, T.A. Lograsso, C.C.H. Lo, A.O. Pecharsky, J.R. Morris, Y. Ye, K.A. Gschneidner Jr., A.J. Slager, Mechanical properties of single crystal YAg, Acta Mater. 52 (2004) 4033–4040.
[44] H. Xing, A. Dong, J. Huang, J. Zhang, B. Sun, Revisiting intrinsic brittleness and deformation behavior of B2 NiAl intermetallic compound: A first-principles study, J. Mater. Sci. Technol. 34 (2018) 620–626.
[45] G.H. Cao, D. Shechtman, D.M. Wu, A.T. Becker, L.S. Chumbley, T.A. Lograsso , A.M. Russell, K.A. Gschneidner Jr., Determination of slip systems and their relation to the high ductility and fracture toughness of the B2 DyCu intermetallic

compound, Acta Mater. 55 (2007) 3765–3770.
[46] J.D. Cotton, M.J. Kaufman, R.D. Noebe, A simplified method for determining the number of independent slip systems in crystals, Scripta Mater. 25 (1991) 2395-2398.
[47] T.M. Pollock, D.C. Lu, X. Shi, K. Eow, A comparative analysis of low temperature deformation in B2 aluminides, Mater. Sci. Eng. A 317 (2001) 241–248.
[48] J. Yang, X. Wang, C. Dong, H. Fu, Thermomechanical instability and deformation behavior of βo(ω) phase region in a Ti-43Al-8Nb-0.2W-0.2B alloy under high-temperature rotary-bending fatigue, Int. J. Fatigue 163 (2022) 106933.
[49] A.V. Kartavykh, E.A. Asnis, N.V. Piskun, I.I. Statkevich, M.V. Gorshenkov, A.V. Korotitskiy, Room-temperature tensile properties of float-zone processed β-stabilized γ-TiAl(Nb,Cr,Zr) intermetallic, Mater. Lett. 188 (2017) 88–91.
[50] H. Liu, Z. Li, F. Gao, Y. Liu, Q. Wang, High tensile ductility and strength in the Ti-42Al-6V-1Cr alloy, J. Alloy Compd. 698 (2017) 898-905.
[51] X. Xu, H. Ding, H. Huang, H. Liang, S. Kawk, R. Chen, J. Guo, H. Fu, Role of growth rate on microstructure evolution, element distribution and nanohardness of phases in directionally solidified multiphase high-Nb TiAl alloy, J. Mater. Res. Technol. 14 (2021) 2884-2896.
[52] M.A. Morris, Y.G. Li, Deformation mechanisms and slip transfer in a Ti-44A1-2Mo alloy, Mater. Sci. Eng. A 197 (1995) 133-145.
[53] C. Qiu, Y. Liu, L. Huang, W. Zhang, Y. He, B. Huang, Tuning mechanical properties for β(B2)-containing TiAl intermetallics, T. Nonferr. Metal Soc. 22 (2012) 2593-2603.
[54] A. Misra, R. Gibala, Slip Transfer and Dislocation Nucleation Processes in Multiphase Ordered Ni-Fe-Al Alloys, Metallurgical and Materials Transactions A, 30 (1999) 991-1001.
[55] J.C. Williams, G. Garmong, Microstructural studies of a Ni-W directionally solidified eutectic composite, Metallurgical Transactions A, 6A (1975) 1699-1709.
[56] H. Song, X. Xu, H. Ding, X. Zhang, R. Chen, J. Guo, H. Fu, Microstructure and nanomechanical behavior of individual phase in β-solidifying Ti-43Al-5Nb-3.5Cr-1Zr alloy J. Mater. Res. Technol. 18 (2022) 1081-1091.
[57] H. Zhu, D.Y. Seo, K. Maruyama, Strengthening of lamellar TiAl alloys by precipitation bands of ω_o particles, Mater. Sci. Eng. A 510-511 (2009) 14-19.
[58] J. Beddoes, D.Y. Seo, W.R. Chen, L. Zhao, Relationship between tensile and primary creep properties of near γ-TiAl intermetallics, Intermetallics 9 (2001) 915-922.
[59] M.H. Yoo, A. Hishinuma, Deformation Twinning in TiAl: Effects of Defect Clustering, Met. Mater. 3 (1997) 65-74.
[60] W.J. Zhang, F. Appel, Effect of Al content and Nb addition on the strength and fault energy of TiAl alloys, Mater. Sci. Eng. A 329-331 (2002) 649-652.
[61] Y. Yuan, H.W. Liu, X.N. Zhao, X.K. Meng, Z.G. Liu, T. Boll, T. Al-Kassab,

Dissociation of super-dislocations and the stacking fault energy in TiAl based alloys with Nb-doping, Phys. Lett. A 358 (2006) 231-235.
[62] G. Shiflet, J. Van der Merwe, The role of structural ledges at phase boundaries – II. Fcc-bcc interfaces in nishiyama-wasserman orientation, Acta Metall. Mater. 42 (1994) 1189–1198.
[63] R.F. Zhang, J. Wang, I.J. Beyerlein, T.C. Germann, Dislocation nucleation mechanisms from fcc/bcc incoherent interfaces, Scripta Mater. 65 (2011) 1022–1025.
[64] R.G. Hoagland, R.J. Kurtz, C.H. Henager Jr., Slip resistance of interfaces and the strength of metallic multilayer composites, Scripta Mater. 50 (2004) 775–779.
[65] D. Choudhuri, B. Gwalani, S. Gorsse, M. Komarasamy, S.A. Mantri, S.G. Srinivasan, R.S. Mishra, R. Banerjee, Enhancing strength and strain hardenability via deformation twinning in fcc-based high entropy alloys reinforced with intermetallic compounds, Acta Mater. 165 (2019) 420-430.
[66] A.H. Cottrell, B.A. Bilby, LX, A mechanism for the growth of deformation twins in crystals, Lond. Edinb. Dublin Philos. Mag. J. Sci. 42 (1951) 573–581.
[67] D. Choudhuri, Srivilliputhur G. Srinivasan, Rajiv S. Mishra, Deformation of lamellar FCC-B2 nanostructures containing Kurdjumov-Sachs interfaces: Relation between interfacial structure and plasticity, Int. J. Plasticity. 125 (2020) 191–209.
[68] X. Gao, Y. Lu, B. Zhang, N. Liang, G. Wu, G. Sha, J. Liu, Y. Zhao, Microstructural origins of high strength and high ductility in an AlCoCrFeNi2.1 eutectic high-entropy alloy, Acta Mater. 141 (2017) 59-66.